

Light localization transition in three-dimensional subrandom arrays

F. Sgrignuoli¹ and L. Dal Negro^{1,2,3,*}

¹*Department of Electrical and Computer Engineering & Photonics Center,
Boston University, 8 Saint Mary's Street, Boston, Massachusetts 02215, USA*

²*Division of Material Science and Engineering, Boston University,
15 Saint Mary's Street, Brookline, Massachusetts 02446, USA*

³*Department of Physics, Boston University, 590 Commonwealth Avenue, Boston, Massachusetts 02215, USA*

We demonstrate a delocalization-localization transition of electromagnetic waves in three-dimensional arrays of electric dipoles generated from subrandom sequences. These systems offer unique opportunities for the design of novel classes of complex media with enhanced localization properties. Specifically, we solve the multiple scattering problem using the Green's matrix spectral theory for aperiodic systems based on Halton, Sobol, and stochastic Latin-Hypercube sequences. By studying the Thouless number and the level spacing statistics of the electromagnetic resonances at different scattering density we demonstrate a clear transition into light localization for the deterministic Halton and Sobol structures. On the other hand, no localization transition was observed in the Latin-Hypercube array, whose behavior resembles instead the one of uniform random media. Our findings establish a connection between light localization and subrandom aperiodic order and provide a novel strategy to design three-dimensional aperiodic structures with strong light-matter interaction.

I. INTRODUCTION

The near-field dipole-dipole coupling between randomly located scatterers is considered one of the main reasons preventing the localization of vector waves in three-dimensional (3D) disordered systems [1, 2]. Due to the uncorrelated nature of the uniform disorder model [3–6], localization of light is predicted to occur only when a strong magnetic field is applied to a 3D ensemble of two-level atoms [7–9]. Moreover, uniform random (UR) systems lack efficient design protocols, often limiting their applications to optical design engineering [10, 11]. To deal with these problems, novel strategies have been developed to localize electromagnetic fields based on aperiodic order in combination with defects engineering [12] and tailored disorder [13]. More recently, it has been shown that aperiodic systems that leverage flat-band physics [14, 15] or deterministic aperiodic geometries [16, 17] can support a delocalization-localization transition (DLT).

In the present work, we study light localization in aperiodic systems generated from subrandom sequences and we demonstrate 3D localization of electromagnetic vector waves with distinctive DLT behavior. Subrandom sequences fill a d -dimensional space more uniformly compared to uncorrelated random ones [18–20] and they are extensively used in statistical sampling theory where they provide superior accuracy and convergence properties [21, 22]. Interestingly, we show that the mathematics of subrandom sequences offers unique opportunities for the design of a novel class of complex media with enhanced light-matter interaction properties with respect to standard UR systems. Specifically, using the rigorous

dyadic Green's matrix spectral method we study the light localization properties of 3D arrays of electric dipoles geometrically arranged according to the Halton, Sobol, and Latin-Hypercube (LH) subrandom sequences. By performing a scaling analysis of the Thouless number [23] and by evaluating the first-neighbor level spacing statistics of the complex Green's matrix eigenvalues, we observe clear signatures of a DLT of electromagnetic waves in the Halton and Sobol configurations, which we found to be hyperuniform deterministic structures. As a result, this localization mechanism is completely different from the Anderson localization model that relies on uncorrelated disorder [3–5]. In fact, we discover that the localization transition in subrandom hyperuniform media is described by a level spacing statistics that does not follow the Ginibre's ensemble of random matrix theory and does not exhibit Poisson statistics at large scattering density. Instead, we find that the probability density function of the level spacing statistics of the Halton and Sobol configurations is well-reproduced by the Gaussian unitary ensemble (GUE) of random matrices in the diffusion regime and by an inverse power law scaling in the localization regime.

On the other hand, we find that the structures generated by the Latin-Hypercube stochastic algorithm are not hyperuniform and do not show any signature of vector waves localization. By systematically comparing both the structural properties, up to the fourth-level correlation order, and the spectral properties of subrandom media with the ones of uniform random structures we attribute the observed localization behavior to the following structural features: (i) the presence of a nearest-neighbor distance probability density function (NNDPDF) with strongly suppressed amplitude for closely separated scattering dipoles compared to the traditional Rayleigh probability density function that describes homogeneous Poisson point processes [24]; (ii)

* dalnegro@bu.edu

the inhibition of long-wavelength density fluctuations. Importantly, these distinctively geometrical characteristics reduce the possible excitation of proximity resonances, which are “dark” sub-radiant modes localized over just few scatterers [25]. In turn, this helps reducing the near-field mediated dipole-dipole interactions, which have been recently identified as key contributions that prevent the occurrence of light localization in 3D uniform random media [26].

II. GEOMETRICAL PROPERTIES OF LOW DISCREPANCY SEQUENCES

The three-dimensional scattering media considered in this work have been designed using the theory of subrandom sequences. This theory is concerned with point sets and sequences having a uniform distribution inside a real interval, such as the distribution of the fractional parts of certain sequences of real numbers $\{x_n\} = x_n - [x_n]$ in the unit interval $I = [0, 1)$. Here $[x_n]$ denotes integer part of x_n , which is the greatest integer smaller or equal to x_n . The fundamental notion is the one of an equidistributed sequence, or a sequence uniformly distributed modulo one, and abbreviated u.d. mod(1). A sequence x_n of real numbers is said to be u.d. mod(1) when the proportion of terms falling inside any half-open sub-interval of I is proportional to the length of that interval. More formally, x_n is said to be u.d. mod(1) if it satisfies the relation:

$$\lim_{N \rightarrow \infty} \frac{A([a, b); N)}{N} = b - a \quad (1)$$

for every pair of real numbers a and b with $0 \leq a < b \leq 1$, where $A([a, b); N)$ denotes the number of terms x_n with $1 \leq n \leq N$ for which the fractional parts of x_n belong to the interval $[a, b)$ [19]. Informally, this definition means that a number sequence x_n is u.d. mod(1) if every half-open sub-interval of I eventually contains its “proper share” of fractional parts.

A central theorem in the theory of equidistributed sequences is the Weyl criterion that provides the necessary and sufficient condition for a general sequence x_n to be u.d. mod(1) in term of the asymptotic behavior of the corresponding exponential sum. The Weyl’s theorem [19], which can be generalized in any dimension, states that an arbitrary sequence x_n of real numbers is u.d. mod(1) if and only if:

$$\lim_{N \rightarrow \infty} \frac{1}{N} \sum_{n=1}^N e^{2\pi i q x_n} = 0 \quad (2)$$

for all integers $q \neq 0$. We note that the trigonometric sum appearing above coincides with the array factor of kinematic diffraction theory. In particular, its squared modulus is proportional to the far-field diffracted intensity from an array of point scatterers with coordinates

x_n . Therefore, Weyl’s theorem implies that large-scale arrays of point scatterers that form a u.d. mod(1) sequence strongly suppress far-field scattering radiation everywhere, except along the forward direction.

The degree of uniformity of equidistributed sequences is quantified by the mathematical concept of discrepancy. For a one-dimensional sequence x_n of N real elements, the discrepancy $D_N = D_N(x_1, \dots, x_n)$ is defined by [19]:

$$D_N = \sup_{0 \leq a < b \leq 1} \left| \frac{A([a, b); N)}{N} - (b - a) \right| \quad (3)$$

For any sequence of N numbers, we have: $1/N \leq D_N \leq 1$. Clearly, the discrepancy D_N of a sequence x_n will be low if the fraction of points falling into an arbitrary subset of the unit interval is close to be proportional to the length of the interval. An important theorem establishes that a sequence x_n is u.d. mod(1) if and only if $\lim_{N \rightarrow \infty} D_N = 0$ [18], thus proving a fundamental equivalence between uniform sequences mod(1) and zero-discrepancy sequences. Finite-length sequences with such asymptotic property are often referred to as subrandom, low-discrepancy, or quasirandom sequences. They differ substantially from traditional random or pseudorandom sequences, such as the ones utilized in random number generators. In fact, while pseudorandom generators uniformly produce outputs in such a way that each trial has the same probability of falling on equal sub-intervals, subrandom sequences are constrained by the low-discrepancy requirement and each point is generated in a highly correlated manner: the next point “knows” where the previous points are located [18]. As a result, subrandom sequences cover a given range of interest more quickly and more evenly than randomly generated numbers (see also Fig 1) [18, 19]. For this reason, subrandom sequences are extensively used in statistical modeling techniques, such as the quasi-Monte Carlo method [21, 22], where they provide better accuracy and faster numerical convergences [18–22]. Interestingly, the elements of subrandom sequences can be generated either in a deterministic fashion, as in the case of the Halton and Sobol sequences, or by a stochastic algorithm, as in the case of the Latin Hypercube sequence.

The principal example of a subrandom sequence is provided by the van der Corput sequence, which represents the fundamental building block for the construction of many others [19]. It is defined by reversing the base b representation of the number n , as explained below. Let $b \geq 2$ be a positive integer and $\mathbb{Z}_b = \{0, 1, \dots, b-1\}$ the least residue system of modulo b . Then, every positive integer $n \geq 0$ has a unique expansion in base b :

$$n = \sum_{k=0}^{m-1} a_k(n) b^k \quad (4)$$

where $a_k(n) \in \mathbb{Z}_b$ and m is the smallest integer such that $a_k(n) = 0$ for all $j > m$ [27]. To define the van der Corput we have to introduce the so-called “radical

inverse function” [19]. For an integer $b \geq 2$, consider the expansion (4) with $n \in \mathbb{N}$. The function $\phi_b : \mathbb{N} \rightarrow [0, 1)$ defined as:

$$\phi_b(n) = \sum_{k=0}^{m-1} a_k(n)b^{-k-1} \quad (5)$$

is the radical inverse function in base b . In reversing the number representation this function makes sure that its values lie in the $(0, 1)$ interval. Moreover, $\phi_b(n)$ can be obtained from n by a symmetric reflection of the expansion (4) with respect to the decimal point. The sequence with terms $x_n = \phi_b(n)$ is the base- b van der Corput sequence, where $b > 1$ is a fixed prime number [19]. This sequence has a discrepancy that scales with the number of elements N as $\sim \ln(N)/N$ [19].

The Halton sequence is a multi-dimensional extension of the van der Corput sequence. To build the Halton sequence we use the van der Corput sequence with different bases for each spatial dimension. In order to generate the 3D Halton array reported in Fig.1 (a), we have used the sequences $\phi_b(2)$, $\phi_b(3)$, and $\phi_b(5)$ in correspondence to the x -, y -, and z - coordinates of the electric point dipoles [28]. On the other hand, the generation of the deterministic Sobol configuration shown in Fig.1 (b) is more sophisticated and requires to permute the order of the elements of the van der Corput sequence. This procedure relies heavily on number theory and on the properties of primitive polynomials to implement permutations along each dimension [29]. The theoretical underpinnings regarding the generation of Sobol sequence can be found in Ref. [30]. Finally, in Fig.1 (c) we display a realization of an array generated using the stochastic algorithm known as Latin Hypercube sampling [27]. This method of generating subrandom sequences is fundamentally different from the previous ones since it is no longer deterministic. In its implementation, it divides each dimension of space into N equally probable sections and positions the values of a uniform random variable in each row and in each column of the grid. This step is repeated to distribute random samples in all the sections of the grid with the requirement that there must be only one sample in each row and each column of the grid, ensuring that different random samples are never spaced too closely in each dimension [27].

In order to obtain more insights on the structural properties of these novel aperiodic media, we analyzed the probability density function $P(d_1)$ of the nearest-neighbor distance, which is among the most important model utilized in the analysis of spatial point patterns [24]. In Fig.1 (d-f) we report the calculated statistical distributions of the nearest spacing d_1 , normalized by the averaged first neighbor spacing \bar{d}_1 . We found that the Halton and the Sobol configurations are characterized by highly fragmented NNPDF statistics with large amplitude fluctuations, while the $P(d_1)$ of the dipole array generated using the stochastic LH algorithm is essentially indistinguishable from the one of a Poisson point

process. Indeed, in Fig.1 (f) we compare the averaged NNPDF $\langle P(d_1) \rangle_e$, where the subscript e refers to the ensemble average with respect to 1000 different realizations of the disorder, of an LH array (grey-bars) with the analytical result (blue-line) corresponding to a uniform random (UR) array. For uniform random arrays the nearest-neighbor distance is statistically described by the Rayleigh density function [24]:

$$P(d_1) = \frac{d_1}{\sigma^2} e^{-d_1^2/2\sigma^2} \quad (6)$$

for $d_1 \geq 0$ where the variance σ is equal to $\sqrt{1/2\pi\mu}$ and μ is the so-called intensity of the Poisson point process, i.e. the average number of points per unit volume [24]. As shown in Fig. 1, the probability to find electric dipoles with a normalized separation lower than 0.5 is very low in the Halton and Sobol arrangements, while the $\langle P(d_1) \rangle_e$ of the LH, which is well described by the Rayleigh distribution, is significantly larger. This distinctive structural difference has a dramatic effect on the strength of the dipole-dipole coupling term, which scales proportionally to $1/r_{ij}^3$ (black-lines in Figs. 1 (d-f)) as well as on the light localization properties of the arrays. In fact, as it will be shown later in the manuscript, light localization occurs in the three-dimensional Halton and Sobol arrays but not in LH or UR structures.

In order to further characterize the structural properties of subrandom arrays we have evaluated the number variance, skewness, and excess (or kurtosis), which are higher-order correlations functions [31, 32]. Indeed, each of these statistical measures can be defined in terms of the moments

$$\mu_j = \left\langle \left(n - \langle n \rangle \right)^j \right\rangle \quad (7)$$

where n is the number of elements in an interval of length L and $\langle \dots \rangle$ represents an average taken over many such intervals throughout the entire system [31, 32]. In particular, the number variance μ_2 is a measure of two-point correlations and enables the identification of the hyperuniform behavior of arbitrary point patterns. Hyperuniformity, a concept introduced by S. Torquato and F. H. Stillinger [33], is a correlated state of matter characterized by the suppression of long-wavelength density fluctuations [34]. This condition leads to the vanishing of the structure factor $S(\mathbf{k}) \rightarrow 0$ in the limit $\mathbf{k} \rightarrow 0$ [34]. Equivalently in 3D structures, hyperuniform systems are characterized by considering the scaling of the fluctuations of the number of points N_R contained within a spherical window of radius R , quantified by the growth of the variance $\mu_2 = \langle N_R^2 \rangle - \langle N_R \rangle^2$ with respect to R . Specifically, a point pattern in d Euclidean dimensions is hyperuniform if μ_2 grows slower than R^d . This feature is clearly reported in Figs.1 (g) and (h) where the density fluctuations of the Halton (green-diamond markers) and Sobol (red-diamond markers) scale proportionally to R^2 (black-dashed line fits), demonstrating their

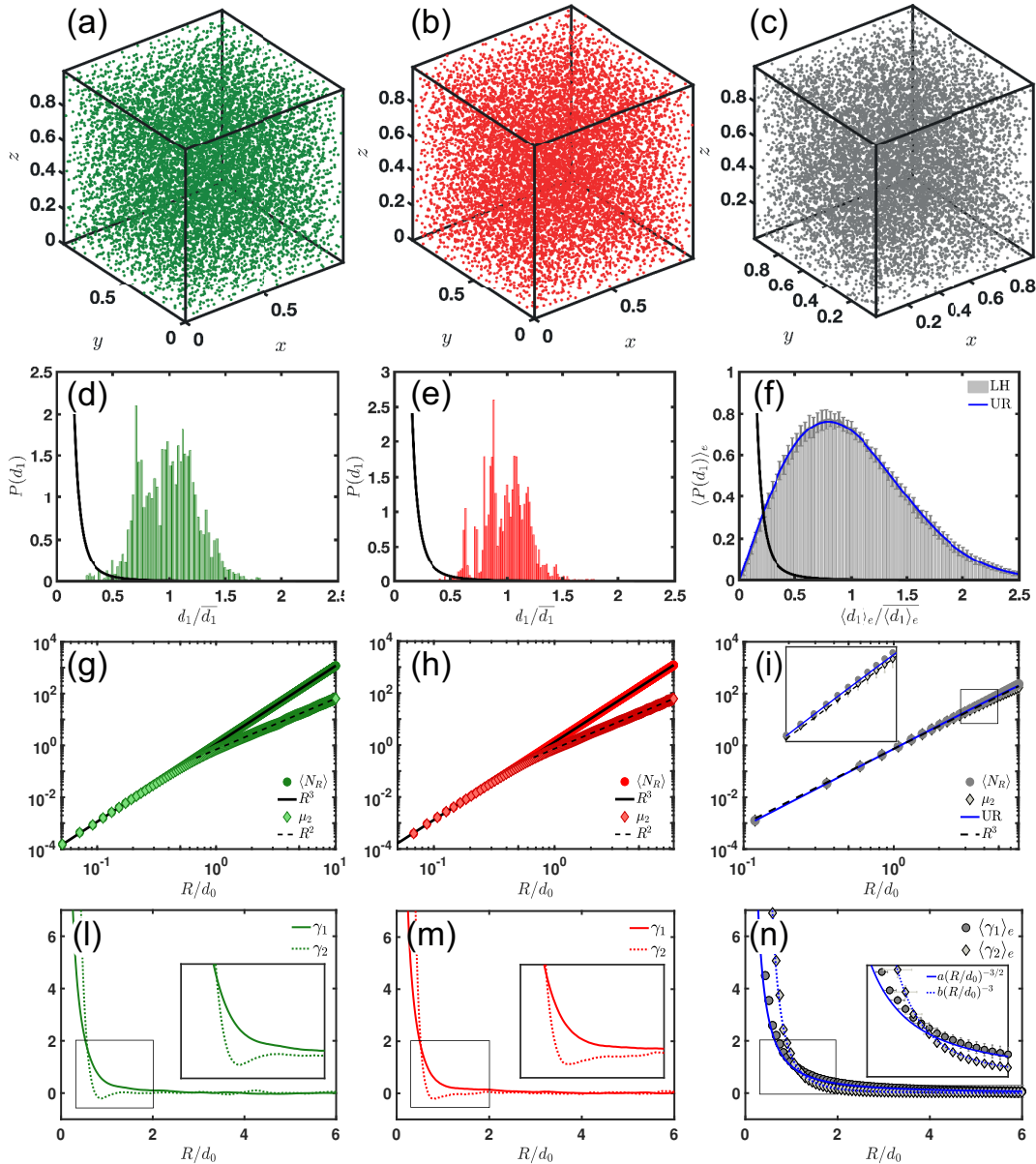


FIG. 1. (a-c) 10^4 electric point dipoles spatially distributed by following the Halton (green-points), Sobol (red-points), and latin hypercube (grey-points) subrandom sequences. (d-f) Nearest-neighbor distance probability density function of the point patterns reported on top of each panels. Panel (f) compares the Rayleigh density function, which describes the nearest-neighbor distance distribution of uniform random (UR) point processes [24], with the averaged NNDPDF of the LH subrandom sequence. The average is performed with respect to 1000 different LH realizations. The continuous black lines identify the decay behavior of the dipole-dipole interaction term that it is proportional to $1/r_{ij}^3$. The scaling of the number of variance $\mu_2 = \langle N(R)^2 \rangle - \langle N(R) \rangle^2$ of 10^4 particles arranged by following the Halton, Sobol, and LH subrandom sequence within a spherical observation window of radius R is reported in panels (g-i), respectively. Panel (i) displays in blue line the average value of the μ_2 two-point correlation function performed over 2000 different UR realizations. Higher-order correlations functions γ_1 and γ_2 of the Halton (l), Sobol (m), and LH (n) arrays. Panel (n) displays the analytical trends of the skewness and excess of uncorrelated Poisson processes in continuous and dotted blue lines, respectively. The error bars of panels (f), (i), and (n) are the statistical errors evaluated with respect to 2000 different realizations of LH point patterns.

hyperuniform nature. On the other hand, in Fig.1 (i) we compare the ensemble averaged (over 1000 stochastic realizations) density fluctuations of the arrays generated according to the LH algorithm (gray-markers) and of a traditional Poisson point process (blue-line). In both

cases we show that the number variance grows with the volume of the spherical window instead with surface, *i.e.* $\mu_2 \propto R^3$ (black-dashed line fit), indicating that UR and LH structures are not hyperuniform (see also the inset of Fig 1 (i)). Hyperuniform patterns arise in a variety of bi-

ological, mathematical, and physical contexts, which includes glass formations [35], colloidal packing and hard-sphere packing [36–38], avian retina [39], immune systems [40], large-scale observations of the Universe [41], and in the engineering of novel photonic devices [42–45], to cite a few. The present work adds another piece to this puzzle, showing that aperiodic scattering 3D media based on deterministic subrandomness are also hyperuniform.

Let now discuss the higher-order correlations. The γ_1 and the γ_2 functions are defined in terms of the moments (7) as [31, 32]:

$$\gamma_1 = \mu_3 \mu_2^{-3/2} \quad \gamma_2 = \mu_4 \mu_2^{-2} - 3 \quad (8)$$

where μ_3 and μ_4 express the 3-level and 4-level correlations, respectively. These high-order correlations functions are reported in Fig. 1 (l-n) and display, as expected, a very different behavior in the Halton (panel l) and Sobol (panel m) configurations with respect to the LH one (panel n), that was averaged over 2000 different relations. Differently from the uncorrelated Poisson point process (continuous and dotted blue lines in Fig. 1 (n)), the Halton and Sobol subrandom arrays are characterized by a skewness and an excess that goes to zero in the $R/d_0 < 1$ range. This difference is attributed to intrinsic higher-order correlation effects [32]. Moreover, γ_1 and γ_2 go to zero for all the arrays when $R/d_0 \geq 1$. The approach to zero, however, is faster for the Halton and Sobol arrays demonstrating the effects of third- and fourth-order structural correlations [32]. On the other hand, Fig. 1 (n) shows that the LH array has no structural correlations up to the fourth-level correlation order. Indeed, both their higher-order correlations functions nicely match the analytical expressions $\gamma_1 = a(R/d_0)^{-3/2}$ and $\gamma_2 = b(R/d_0)^{-3}$ that are valid for an uncorrelated Poisson process. Here the coefficients a and b are equal to $1/2\sqrt{\rho}$ and $1/3\rho$, respectively. The parameter ρ is the scatterers density N/V , while N and V are the number of point and the volume, respectively.

III. SPECTRAL PROPERTIES OF LOW DISCREPANCY SEQUENCES

We now investigate the spectral and wave localization properties of 3D electric dipole arrays generated according to Halton, Sobol, and LH subrandom sequences. Multiple scattering effects in these novel scattering media are studied by analyzing the properties of the Green’s matrix with elements [46, 47]:

$$G_{ij} = i \left(\delta_{ij} + \tilde{G}_{ij} \right) \quad (9)$$

where \tilde{G}_{ij} has the form:

$$\tilde{G}_{ij} = \frac{3}{2} (1 - \delta_{ij}) \frac{e^{ik_0 r_{ij}}}{ik_0 r_{ij}} \left\{ \left[\mathbf{U} - \hat{\mathbf{r}}_{ij} \hat{\mathbf{r}}_{ij} \right] - \left(\mathbf{U} - 3\hat{\mathbf{r}}_{ij} \hat{\mathbf{r}}_{ij} \right) \left[\frac{1}{(k_0 r_{ij})^2} + \frac{1}{ik_0 r_{ij}} \right] \right\} \quad (10)$$

when $i \neq j$ and 0 for $i = j$. k_0 is the wavevector of light, the integer indexes $i, j \in 1, \dots, N$ refer to different particles, \mathbf{U} is the 3×3 identity matrix, $\hat{\mathbf{r}}_{ij}$ is the unit vector position from the i -th and j -th scatterer while r_{ij} identifies its magnitude. The real and the imaginary part of the complex eigenvalues Λ_n ($n \in 1, 2, \dots, 3N$) of matrix (9) are related to the detuned scattering frequency ($\omega_0 - \omega$) and to the scattering decay Γ_n both normalized to resonant width Γ_0 of a bare dipole [46, 47]. This spectral approach accounts for all the multiple scattering orders of arbitrary arrays of electric scattering point dipoles, so that the multiple scattering process is treated exactly. In addition, this method separates the structural properties of an arbitrary scattering systems from their material characteristics. Therefore, the predictions of the Green’s approach should be considered “universal” in the limit of electric dipole scatterers that is valid for particles with small size parameter $x = k\hat{r}$ (k is the wavenumber and \hat{r} is the particle radius). However, this method can also be extended to include higher-order multipolar resonances [48], which are outside the scope of the present work. The study of the spectral properties of the non-Hermitian Green matrix (9) is an excellent approximation in the case of atom clouds or of metal/dielectric particles whose size is much smaller than the wavelength [49]. Cold atoms might represent a suitable alternative to dielectric materials to experimentally demonstrate light localization in 3D environments. Indeed, even though state of the art lithographic techniques allowed the realizations of complex three-dimensional polymeric photonic inverted networks [50–52], the fabrication of *deterministic* volumetric structures embedded in a polymer matrix is one of the key challenges of materials science today. On the other hand, quantum-gas microscopes [53] enabled the engineering of one [54], two [55], and even three-dimensional [56–59] optical potentials with arbitrary shape while keeping single-atom control to simulate models from condensed matter physics in high controlled environments. Therefore, novel 3D optical scattering potentials based on engineered subrandom sequences could be effectively achieved [59], providing suitable platforms to experimentally demonstrate the results of this paper.

To demonstrate light localization, we have analyzed the scaling of the minimum value of Thouless conductance and the level spacing crossover from level repulsion to level clustering as a function of the scattering density ρ/k_0^3 . Here k_0 is the vacuum wavenumber. Specifically, we have studied these spectral properties by numerically diagonalizing the $3N \times 3N$ Green’s matrix (9) that, in the present manuscript, can describe the propagation of light in 3D atomic clouds with subrandom geometries based on the Halton, Sobol, and the LH sequences.

At low scattering density ($\rho/k_0^3 = 0.001$), all the investigated systems are in the delocalized regime. Their eigenvalue distributions, color coded according to the \log_{10} values of the modal spatial extent (MSE) [60], do not show any particular features. While Figs. 2 (a) and (b) display a very similar distribution of complex scat-

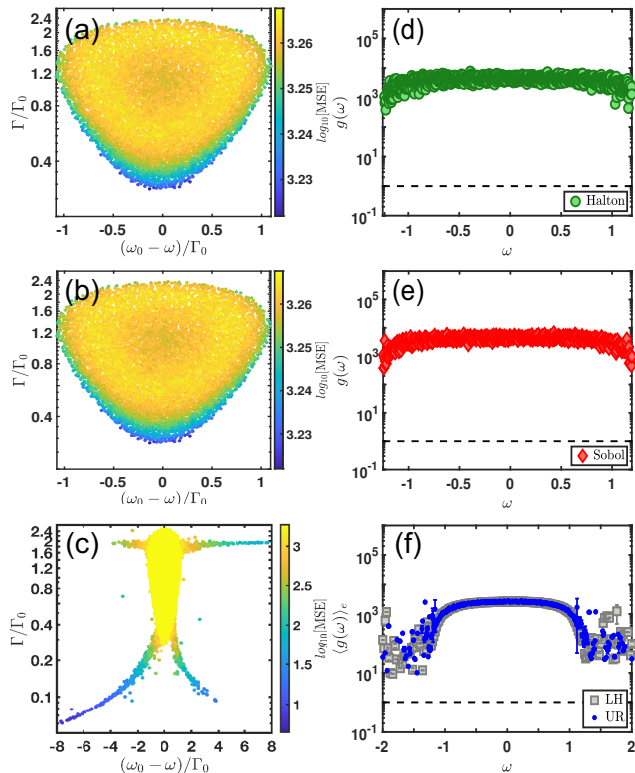


FIG. 2. Eigenvalues of the electric Green's matrix (9) in the low scattering regime ($\rho/k_0^3 = 0.001$) of the Halton (a), Sobol (b), and LH (c) subrandom sequence, respectively. Panels (d-f) show the corresponding Thouless numbers as a function of the frequency ω . Panel (f) compares the averaged Thouless number $\langle g(\omega) \rangle_e$ (the subscript e refers to ensemble average with respect to 100 different realizations) of the LH sequence (square-gray markers) with respect to the traditional UR distribution (blue-dots). The error bars are the standard deviations. The dashed-black lines identify the threshold of the diffusion-localization transition.

tering resonances delocalized across their 3D geometrical supports (note their very high MSE values), the eigenvalue distributions of the latin hypercube configurations resemble the ones of the standard UR system [1, 2]. These results are corroborated by the behavior of the Thouless number g as a function of the frequency ω evaluated as [16]:

$$g(\omega) = \frac{\overline{\delta\omega}}{\overline{\Delta\omega}} = \frac{\overline{(1/\Im[\Lambda_n])^{-1}}}{\Re[\Lambda_n] - \Re[\Lambda_{n-1}]} \quad (11)$$

Specifically, we have subdivided the range of the resonance frequencies in 500 equispaced intervals and we have calculated the ratio between the average value of the dimensionless lifetimes and the average spacing of nearest dimensionless resonant frequencies for each frequency sub-intervals. The symbol $\{\dots\}$ in Eq.(11) indicates this average operation, while the frequency ω is

the central frequency of each sub-interval used to sample the $\Re[\Lambda_n]$ [16]. As expected, we found that at low scattering density the Thouless number is always larger than one in Fig. 2 (d-f) for all the analyzed clouds. Moreover, the averaged Thouless number $\langle g(\omega) \rangle_e$ of the LH sequence (square-gray markers) is very similar to the averaged Thouless number of traditional UR systems (blue-dots), as shown in Fig. 2 (f). The subscript e refers to ensemble average with respect to 100 different Poisson and latin-hypercube different realizations.

On the other hand, at large scattering density $\rho/k_0^3 = 0.5$ light interacts differently with the two deterministic and hyperuniform 3D subrandom arrays. As shown in Fig. 3, while the stochastic LH subrandom configuration shows a delocalized regime dominated by proximity resonances (dark-grey markers in Fig 3 (c)), the Halton and the Sobol deterministic configurations are characterized by (i) the formation of spectral gaps,

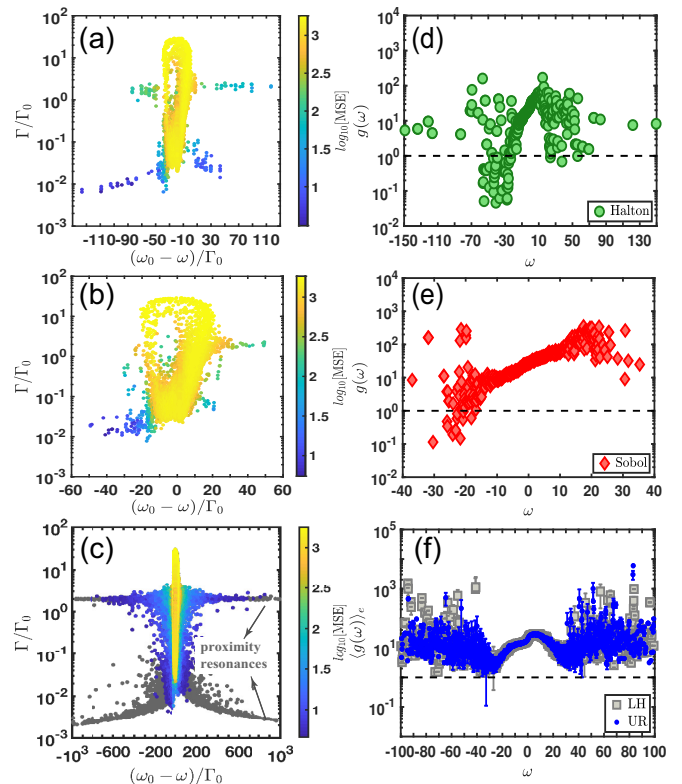


FIG. 3. Eigenvalues of the electric Green's matrix (9) are shown by points on the complex plane for 2000 electric dipoles arranged by following the Halton (a), Sobol (b), and LH (c) subrandom sequence. These complex eigenvalue distributions are produced when ρ/k_0^3 is equal to 0.5. Panels (d-f) show the corresponding Thouless conductances as a function of the frequency ω . Panel (f) compares the averaged Thouless conductance $\langle g(\omega) \rangle_e$ (the subscript e refers to ensemble average with respect to 100 different realizations) of the LH sequence (square-gray markers) with respect to the traditional UR distribution (blue-points). The error bars are the standard deviations. The dashed-black lines identify the threshold of the diffusion-localization transition.

proximity resonances, (iii) and a Thouless number lower than one. This finding is a clear signature that such systems can support localized vector waves in all dimensions. The absence of sub-radiant dark resonances, attributed to the previously discussed correlation properties of the Halton and Sobol arrays, is reflected in the formation of clear spectral gaps in their distributions of complex poles. These features reduce drastically the near-field interaction term in eq. (10) allowing 3D light localization to appear in such systems. On the contrary, this scenario does not occur in traditional UR systems and in the structures based on LH sequences. In these cases, vector wave localization is inhibited due to the strong dipole-dipole interactions resulting from the close particles encounters described by the Rayleigh first-neighbor distance probability distribution, as shown in Fig. 1 (f).

In order to get more insights on the discovered DLT, we have analyzed the scaling of the minimum value of

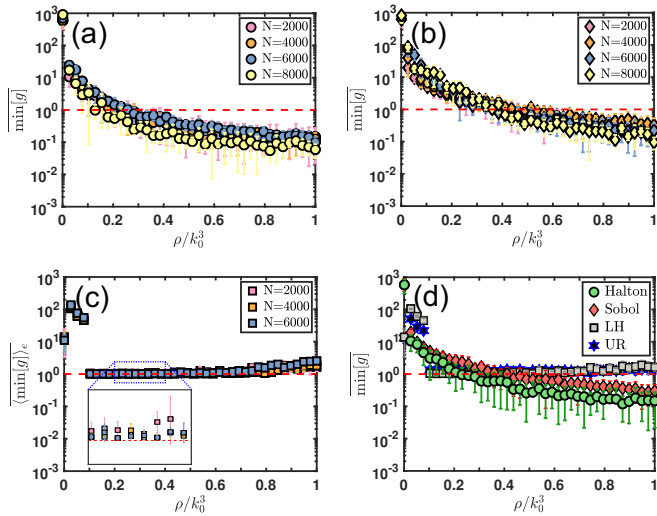


FIG. 4. Panels (a-c) display the scaling of the minimum value of the Thouless conductance as a function of ρ/k_0^3 for Halton (a), Sobol (b), and LH (c) subrandom sequence, respectively. The pastel rose, orange, blue, and yellow markers refer to 2000, 4000, 6000, and 8000 electric dipoles, respectively. The error bars in panel (c) are the standard deviations related to the different disorder realizations. The number of independent configurations were adjusted to ensure a total of at least 2×10^5 eigenvalues for each N . (d) Minimum of the Thouless conductance as a function of the scattering strength ρ/k_0^3 of Halton (green circle-markers), Sobol (red diamond-markers), and LH (grey square-markers) as compared to the uniform random configuration ensemble averaged over 100 different disordered realizations (blue-black pentagrams markers). 100 different realizations were considered also for the LH sequence. The error bars takes into account the different frequency resolutions (see text for more details) used during the Thouless conductance calculations for the Halton and Sobol configurations. In the LH and UR sequences the error bars are statistical errors related to the different disorder realizations. Moreover, the proximity resonances were removed during this analysis.

the Thouless number of arrays with 2000 (pink-markers), 4000 (orange-markers), 6000 (blue-markers), and 8000 (yellow-markers) electric dipoles as a function of the scattering density. The results of this analysis are reported in Fig. 4 (a), (b), and (c) for Halton, Sobol, and LH clouds, respectively. Specifically, we have evaluated $g = g(\omega)$ by employing eq. (11) for each ρ/k_0^3 value and we have repeated this procedure for different frequency resolutions used in the computation of the Thouless number. Fig. 4 reports their averaged values $\min[g]$ and their standard deviations as error bars. In the LH configuration, we performed also an average with respect to different stochastic realizations. The number of independent realizations were adjusted to ensure a total of at least 2×10^5 eigenvalues for each N . The scaling of $\min[g]$ as a function of the scattering density exhibits a clear DLT for the two deterministic, aperiodic, and hyperuniform Halton and Sobol structures. Localization begins to take place at ρ/k_0^3 approximately equal to 0.25 and 0.4 in the Halton and Sobol configurations, respectively. In contrast, light localization never appears in dipole arrays generated by LH stochastic sequences (see inset of Fig. 4c). Finally, in Fig. 4 (d) we compare the minimum of the Thouless number of the low-discrepancy sequences with the case of traditional random media (pentagram-markers) when $N=2000$. Consistently with the first-neighbor probability distribution, the higher-order correlation analysis, the complex eigenvalues distributions, and the study of the Thouless number, we found that the LH and UR display a very similar behavior. These findings underline a fundamental connection between the structural/geometrical properties of the arrays and their ability/inability to localize electromagnetic waves.

In order to further understand the nature of the discovered localization transitions, we have studied the probability density function of the first-neighbor level spacing statistics of the complex Green's matrix eigenvalues $P(\hat{s})$, where $\hat{s} = |\Delta\Lambda| / \langle |\Delta\Lambda| \rangle$ is the nearest-neighbor eigenvalue spacing $|\Delta\Lambda| = |\Lambda_{n+1} - \Lambda_n|$ normalized to the average spacing. It is well-established that the suppression of the level repulsion phenomenon, i.e. $P(\hat{s}) \rightarrow 0$ when $\hat{s} \rightarrow 0$, indicates the transition to localized states in both uniform [7, 61] and non-uniform open-scattering systems [16, 48]. The distributions of level spacing show a clear crossover from level repulsion at low optical density to the absence of level repulsion at large optical density, which is akin to the situation observed in uniform random media under a strong magnetic field [7]. However, despite this similarity, the observed transition into the localized regime presents substantial differences with respect to the UR scenario, indicating that a different localization mechanism governs light interaction in the Halton and Sobol subrandom structures. In fact, we found that at low ρ/k_0^3 , the distribution of the level spacing predicted by the Ginibre's ensemble of random matrices, which describes dissipative UR systems [62], does not well-reproduce the spectral statistics shown in Fig. 5 (a,b). Instead, an excellent agreement was found using the Gaus-

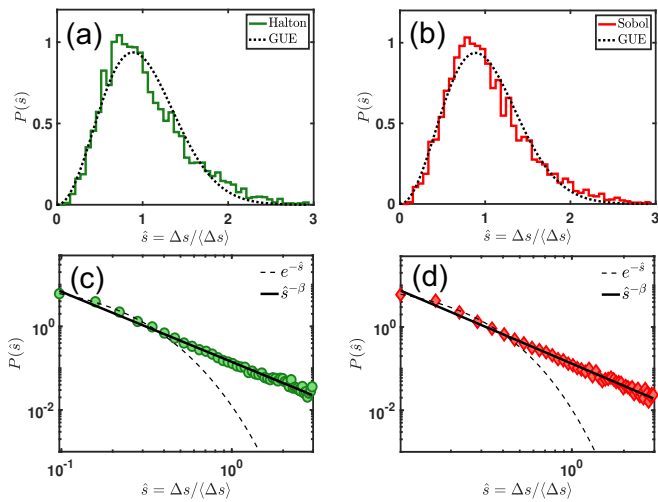


FIG. 5. Probability distribution functions of level spacing statistic of 6000 Green’s matrix eigenvalues for two different scattering regime: $\rho/k_0^3 = 10^{-3}$ (a-b) and $\rho/k_0^3 = 1$ (c-d) for Halton (green) and Sobol (red), respectively. The nearest-neighbor distribution of the eigenvalues of the gaussian unitary ensemble, described by the eq. (12), is displayed for comparison in panels (a-b) with a black-dashed line. Panels (c-d) show that the PDFs of level spacing statistic of the Green’s matrix eigenvalues of Halton and Sobol 3D subrandom point patterns does not follow the traditional Poisson distribution $e^{-\hat{s}}$ (black-dotted lines) but a power-law statistic $\hat{s}^{-\beta}$ (black continuous lines) in the large scattering regime. The values of the fitted β are 1.7 ± 0.1 and 1.8 ± 0.1 in the Halton and Sobol configurations, respectively.

sian unitary ensemble (GUE) formula [31, 63]:

$$P(\hat{s}) = \frac{32}{\pi^2} \hat{s}^2 e^{-4\hat{s}^2/\pi} \quad (12)$$

We emphasize that the black-dashed lines in Fig. 5 (a-b) are not the results of a numerical fitting procedure but are simply obtained by using eq. (12). This distribution falls off quadratically for $\hat{s} \rightarrow 0$ [31, 63], demonstrating that the eigenvalues of the Halton and Sobol exhibit quadratic level repulsion in the low scattering density regime. Interestingly, the GUE distribution (12) has also been discovered in the spacing of the non-trivial zeros of the Riemann’s zeta function [64], whose properties are intimately related to the distribution of prime numbers [65]. Such a discovery motivated the Montgomery’s conjecture [66] that the pair-correlation function of the non-trivial Riemann’s zeros is essentially determined by the properties of random Hermitian matrices. The fundamental connection between the Riemann’s zeros and random unitary matrices may provide a fruitful approach to a proof of the Riemann hypothesis [67]. Interestingly, our findings provide an unexpected connection between the GUE distribution, associated to the distinctive distribution of the Riemann’s zeros, and wave transport (in the low scattering regime) through Sobol and Halton deterministic subrandom structures.

Additionally, at large optical density we observed a substantial deviation (black-dashed lines in Fig. 5 (c-d)) from the Poisson statistics that typically describes non-interacting energy levels [31, 63] in UR systems. In contrast, the level spacing distributions for Halton and Sobol configurations, shown by the green-circle and red-diamond markers in Figs. 5 (c) and (d), are well-reproduced by the inverse power law scaling curves $P(\hat{s}) \sim \hat{s}^{-\beta}$ shown by the continuous black lines, with the exponent β equal to 1.7 ± 0.1 and 1.8 ± 0.1 , respectively. In the context of random matrix theory, it has been demonstrated that this particular distribution is a characteristic of complex systems with multifractal spectra (uncountable sets of hierarchical level clustering) [68, 69]. Moreover, this power-law scaling appears to universally describe the transport physics, with values of the exponent β in the range $0.5 < \beta < 2$, of systems exhibiting anomalous diffusion, *i.e.* systems in which the width of a wavepacket σ^2 increases upon propagation like $t^{2\nu}$ with $\nu \in [0, 1]$ [68, 70]. Specifically, such a behavior was observed in one-dimensional scattering systems characterized by incommensurate sinusoidal modulations, in quasi-periodic Fibonacci structures, and in a family of tight-binding Hamiltonians defined on two-dimensional octagonal quasi-periodic tilings [69, 71, 72]. The exponents β and ν can be related to the average (box-counting) fractal dimension D_0 of the diffusing system through the relation [68, 69, 73]

$$\sigma^2(t) \sim t^{2\nu} = t^{2D_0/d} = t^{2(\beta-1)/d} \quad (13)$$

where d is the system dimensionality. By substituting the numbers obtained from the numerical fits of the data in Fig. 5 (c-d) into eq. (13), we find that the exponent ν is equal to 0.23 ± 0.03 and 0.27 ± 0.07 for the Halton and Sobol configurations, respectively. The fact that ν is lower than 0.5 in both configurations indicates that the propagation of wavepackets through such structures is sub-diffusive, potentially enabling novel sub-diffusive laser structures that leverage deterministic subrandomness as an effective approach to achieve reduced amplification thresholds and footprints compared to traditional random lasers [74]. Interestingly, the behavior that we observed in deterministic subrandom structures closely resembles the electronic transport in 3D weakly disordered systems at the metal-insulator-transition (MIT) where multifractality has been demonstrated [75] with the subdiffusive exponent $\nu = 0.2$ [75–78]. This result redefined the standard picture of localization demonstrating that subdiffusion, which is produced by weak localization effects [79], is an intermediate step between the diffusive and the fully localized regime [78]. By following this interpretation, the reported crossover between level repulsion and level clustering in Fig. 5 can be explained as a transition from a diffusive to a weak-localization regime in which the eigenstates are multifractal and the transport dynamics becomes subdiffusive.

Our findings clearly establish that deterministic subrandom structures strongly reduce dipole-dipole interac-

tions resulting in the reported delocalized-localized transition of vector waves in 3D complex environments.

IV. CONCLUSIONS

The data presented in this manuscript demonstrate that deterministic media based on the Halton and Sobol subrandom sequences enable the localization of electromagnetic waves in three-dimensions. Specifically, by performing a scaling analysis of the Thouless number and by studying the first-neighbor level spacing statistics of the complex Green's matrix eigenvalues, we have established a clear transition from a diffusive to a weak-localization regime, characterized by a power-law level spacing at large optical density and by GUE statistics in the diffusive regime. Moreover, we have also shown that subrandom structures generated by the stochastic Latin-Hypercube sequence do not show any signatures of light localization. By comparing both the structural, up to the fourth-level correlation order, and the scattering properties of subrandom structures in comparison to traditional uniform random ones, we established two properties of primary importance to achieve localization of electromagnetic waves: (i) a marked deviation from a Rayleigh probability distribution for the first-neighbor spacing statistics of UR systems, (ii) the suppression of

the long-wavelength density fluctuations. These structural features lead to the absence of proximity resonances, and a reduction of the dipole-dipole interactions that should not surpass a critical strength in order to guarantee light localization in 3D. Our analysis clearly shows that the strength of the dipole-dipole coupling between vector dipoles is drastically reduced in the Halton and Sobol configurations due to their structural correlation properties. Recent developments in quantum-gas microscopes have allowed the creation of 3D resonant optical traps of arbitrary shapes while keeping single-atom control. These novel techniques may offer a reliable platform to experimentally demonstrate the results of our manuscript.

ACKNOWLEDGMENTS

This research was sponsored by the Army Research Laboratory and was accomplished under Cooperative Agreement Number W911NF-12-2-0023. The views and conclusions contained in this document are those of the authors and should not be interpreted as representing the official policies, either expressed or implied, of the Army Research Laboratory or the U.S. Government. The U.S. Government is authorized to reproduce and distribute reprints for Government purposes notwithstanding any copyright notation herein.

-
- [1] S. E. Skipetrov and I. M. Sokolov, *Absence of Anderson localization of light in a random ensemble of point scatterers*, Phys. Rev. Lett. **112**, 023905 (2014).
 - [2] L. Bellando, A. Gero, E. Akkermans, and R. Kaiser, *Cooperative effects and disorder: A scaling analysis of the spectrum of the effective atomic Hamiltonian*, Phys. Rev. A **90**, 063822 (2014).
 - [3] P. Sheng, *Introduction to wave scattering, localization and mesoscopic phenomena*, Vol. 88 (Springer Science & Business Media, 2006).
 - [4] E. Akkermans and G. Montambaux, *Mesoscopic physics of electrons and photons* (Cambridge university press, 2007).
 - [5] P. W. Anderson, *Absence of diffusion in certain random lattices*, Phys. Rev. **109**, 1492 (1958).
 - [6] D. S. Wiersma, *Disordered photonics*, Nat. Photonics **7**, 188 (2013).
 - [7] S. E. Skipetrov and I. M. Sokolov, *Magnetic-field-driven localization of light in a cold-atom gas*, Phys. Rev. Lett. **114**, 053902 (2015).
 - [8] S. Skipetrov, *Localization transition for light scattering by cold atoms in an external magnetic field*, Phys. Rev. Lett. **121**, 093601 (2018).
 - [9] F. Cottier, A. Cipris, R. Bachelard, and R. Kaiser, *Microscopic and macroscopic signatures of 3D Anderson localization of light*, Phys. Rev. Lett. **123**, 083401 (2019).
 - [10] D. Balestri, M. Petruzzella, S. Checcucci, F. Intonti, N. Caselli, F. Sgrignuoli, F. W. van Otten, A. Fiore, and M. Gurioli, *Mechanical and Electric Control of Photonic Modes in Random Dielectrics*, Adv. Mater. **31**, 1807274 (2019).
 - [11] F. Riboli, N. Caselli, S. Vignolini, F. Intonti, K. Vynck, P. Barthelemy, A. Gerardino, L. Balet, L. H. Li, A. Fiore, et al., *Engineering of light confinement in strongly scattering disordered media*, Nature materials **13**, 720 (2014).
 - [12] B. Freedman, G. Bartal, M. Segev, R. Lifshitz, D. N. Christodoulides, and J. W. Fleischer, *Wave and defect dynamics in nonlinear photonic quasicrystals*, Nature **440**, 1166 (2006).
 - [13] L. Levi, M. Rechtsman, B. Freedman, T. Schwartz, O. Manela, and M. Segev, *Disorder-enhanced transport in photonic quasicrystals*, Science **332**, 1541 (2011).
 - [14] P. Wang, Y. Zheng, X. Chen, C. Huang, Y. V. Kartashov, L. Torner, V. V. Konotop, and F. Ye, *Localization and delocalization of light in photonic moiré lattices*, Nature , 1 (2019).
 - [15] F. Sgrignuoli, M. Röntgen, C. V. Morfonios, P. Schmelcher, and L. Dal Negro, *Compact localized states of open scattering media: a graph decomposition approach for an ab initio design*, Opt. Lett. **44**, 375 (2019).
 - [16] F. Sgrignuoli, R. Wang, F. Pinheiro, and L. Dal Negro, *Localization of scattering resonances in aperiodic Vogel spirals*, Phys. Rev. B **99**, 104202 (2019).
 - [17] L. Dal Negro, R. Wang, and F. Pinheiro, *Structural and spectral properties of deterministic aperiodic optical*

- structures, *Crystals* **6**, 161 (2016).
- [18] H. Niederreiter, *Low-discrepancy and low-dispersion sequences*, *J. Number Theory* **30**, 51 (1988).
- [19] L. Kuipers and H. Niederreiter, *Uniform distribution of sequences* (Courier Corporation, 2012).
- [20] M. D. McKay, R. J. Beckman, and W. J. Conover, *A comparison of three methods for selecting values of input variables in the analysis of output from a computer code*, *Technometrics* **42**, 55 (2000).
- [21] C. Lemieux, *Monte Carlo and Quasi-Monte Carlo Sampling*, Springer Series in Statistics (Springer, Dordrecht, 2009).
- [22] W. J. Morokoff and R. E. Caflisch, *Quasi-monte Carlo integration*, *J. Comput. Phys.* **122**, 218 (1995).
- [23] D. J. Thouless, *Electrons in disordered systems and the theory of localization*, *Phys. Rep.* **13**, 93 (1974).
- [24] J. Illian, A. Penttinen, H. Stoyan, and D. Stoyan, *Statistical analysis and modelling of spatial point patterns*, Vol. 70 (John Wiley & Sons, 2008).
- [25] E. J. Heller, *Quantum proximity resonances*, *Phys. Rev. Lett.* **77**, 4122 (1996).
- [26] S. Skipetrov and I. Sokolov, *Search for Anderson localization of light by cold atoms in a static electric field*, *Phys. Rev. B* **99**, 134201 (2019).
- [27] H. T. Huynh, I. Soumare, *et al.*, *Stochastic simulation and applications in finance with MATLAB programs*, Vol. 633 (John Wiley & Sons, 2011).
- [28] L. Kocis and W. J. Whiten, *Computational investigations of low-discrepancy sequences*, *ACM Trans. Math. Softw.* **23**, 266 (1997).
- [29] S. Joe and F. Y. Kuo, *Remark on algorithm 659: Implementing Sobol's quasirandom sequence generator*, *ACM Trans. Math. Softw.* **29**, 49 (2003).
- [30] I. M. Sobol', *On the distribution of points in a cube and the approximate evaluation of integrals*, *Zhurnal Vychislitel'noi Matematiki i Matematicheskoi Fiziki* **7**, 784 (1967).
- [31] M. L. Mehta, *Random matrices*, Vol. 142 (Elsevier, 2004).
- [32] O. Bohigas, R. U. Haq, and A. Pandey, *Higher-order correlations in spectra of complex systems*, *Phys. Rev. Lett.* **54**, 1645 (1985).
- [33] S. Torquato and F. H. Stillinger, *Local density fluctuations, hyperuniformity, and order metrics*, *Phys. Rev. E* **68**, 041113 (2003).
- [34] S. Torquato, *Hyperuniform states of matter*, *Phys. Rep.* **745**, 1 (2018).
- [35] A. Chremos and J. F. Douglas, *Particle localization and hyperuniformity of polymer-grafted nanoparticle materials*, *Ann. Phys.* **529**, 1600342 (2017).
- [36] R. Dreyfus, Y. Xu, T. Still, L. A. Hough, A. Yodh, and S. Torquato, *Diagnosing hyperuniformity in two-dimensional, disordered, jammed packings of soft spheres*, *Phys. Rev. E* **91**, 012302 (2015).
- [37] A. Donev, F. H. Stillinger, and S. Torquato, *Unexpected density fluctuations in jammed disordered sphere packings*, *Phys. Rev. Lett.* **95**, 090604 (2005).
- [38] C. E. Zachary, Y. Jiao, and S. Torquato, *Hyperuniform long-range correlations are a signature of disordered jammed hard-particle packings*, *Phys. Rev. Lett.* **106**, 178001 (2011).
- [39] Y. Jiao, T. Lau, H. Hatzikirou, M. Meyer-Hermann, J. C. Corbo, and S. Torquato, *Avian photoreceptor patterns represent a disordered hyperuniform solution to a multi-scale packing problem*, *Phys. Rev. E* **89**, 022721 (2014).
- [40] A. Mayer, V. Balasubramanian, T. Mora, and A. M. Walczak, *How a well-adapted immune system is organized*, *Proc. Natl. Acad. Sci. USA* **112**, 5950 (2015).
- [41] L. Pietronero and F. S. Labini, *Statistical physics for cosmic structures*, in *Complexity, Metastability and Nonextensivity* (World Scientific, 2005) pp. 91–101.
- [42] M. Florescu, S. Torquato, and P. J. Steinhardt, *Designer disordered materials with large, complete photonic band gaps*, *Proc. Natl. Acad. Sci. USA* **106**, 20658 (2009).
- [43] W. Man, M. Florescu, E. P. Williamson, Y. He, S. R. Hashemizad, B. Y. Leung, D. R. Liner, S. Torquato, P. M. Chaikin, and P. J. Steinhardt, *Isotropic band gaps and freeform waveguides observed in hyperuniform disordered photonic solids*, *Proc. Natl. Acad. Sci. USA* **110**, 15886 (2013).
- [44] R. Degl'Innocenti, Y. Shah, L. Masini, A. Ronzani, A. Pianti, Y. Ren, D. Jessop, A. Tredicucci, H. E. Beere, and D. A. Ritchie, *Hyperuniform disordered terahertz quantum cascade laser*, *Sci. Rep.* **6**, 19325 (2016).
- [45] S. Gorsky, W. Britton, Y. Chen, J. Montaner, A. Lenef, M. Raukas, and L. Dal Negro, *Engineered hyperuniformity for directional light extraction*, *APL Photonics* **4**, 110801 (2019).
- [46] M. Rusek, A. Orłowski, and J. Mostowski, *Localization of light in three-dimensional random dielectric media*, *Phys. Rev. E* **53**, 4122 (1996).
- [47] A. Lagendijk and B. A. Van Tiggelen, *Resonant multiple scattering of light*, *Phys. Rep.* **270**, 143 (1996).
- [48] L. Dal Negro, Y. Chen, and F. Sgrignuoli, *Aperiodic Photonics of Elliptic Curves*, *Crystals* **9**, 482 (2019).
- [49] C. F. Bohren and D. R. Huffman, *Absorption and scattering of light by small particles* (John Wiley & Sons, 2008).
- [50] N. Muller, J. Haberko, C. Marichy, and F. Scheffold, *Photonic hyperuniform networks obtained by silicon double inversion of polymer templates*, *Optica* **4**, 361 (2017).
- [51] S. Nocentini, D. Martella, C. Parmeggiani, and D. S. Wiersma, *3D Printed Photoresponsive Materials for Photonics*, *Adv. Opt. Mater.* , 1900156 (2019).
- [52] S. Zanotto, F. Sgrignuoli, S. Nocentini, D. Martella, C. Parmeggiani, and D. S. Wiersma, *Multichannel remote polarization control enabled by nanostructured liquid crystalline networks*, *Appl. Phys. Lett.* **114**, 201103 (2019).
- [53] S. Kuhr, *Quantum-gas microscopes: a new tool for cold-atom quantum simulators*, *Natl. Sci. Rev.* **3**, 170 (2016).
- [54] M. Endres, H. Bernien, A. Keesling, H. Levine, E. R. Anschuetz, A. Krajenbrink, C. Senko, V. Vuletic, M. Greiner, and M. D. Lukin, *Atom-by-atom assembly of defect-free one-dimensional cold atom arrays*, *Science* **354**, 1024 (2016).
- [55] D. Barredo, S. De Léséleuc, V. Lienhard, T. Lahaye, and A. Browaeys, *An atom-by-atom assembler of defect-free arbitrary two-dimensional atomic arrays*, *Science* **354**, 1021 (2016).
- [56] M. Greiner, *Ultracold quantum gases in three-dimensional optical lattice potentials*, Ph.D. thesis, lmu (2003).
- [57] Y. Wang, X. Zhang, T. A. Corcovilos, A. Kumar, and D. S. Weiss, *Coherent addressing of individual neutral atoms in a 3D optical lattice*, *Phys. Rev. Lett.* **115**, 043003 (2015).
- [58] K. D. Nelson, X. Li, and D. S. Weiss, *Imaging single atoms in a three-dimensional array*, *Nat. Phys.* **3**, 556

- (2007).
- [59] D. Barredo, V. Lienhard, S. De Leseleuc, T. Lahaye, and A. Browaeys, *Synthetic three-dimensional atomic structures assembled atom by atom*, *Nature* **561**, 79 (2018).
- [60] F. Sgrignuoli, G. Mazzamuto, N. Caselli, F. Intonti, F. S. Cataliotti, M. Gurioli, and C. Toninelli, *Necklace state hallmark in disordered 2D photonic systems*, *ACS Photonics* **2**, 1636 (2015).
- [61] J. M. Escalante and S. E. Skipetrov, *Level spacing statistics for light in two-dimensional disordered photonic crystals*, *Sci. Rep.* **8**, 11569 (2018).
- [62] I. K. Zharekeshv and B. Kramer, *Asymptotics of universal probability of neighboring level spacings at the Anderson transition*, *Phys. Rev. Lett.* **79**, 717 (1997).
- [63] F. Haake, *Quantum signatures of chaos*, in *Quantum Coherence in Mesoscopic Systems* (Springer, 1991) pp. 583–595.
- [64] A. M. Odlyzko, *On the distribution of spacings between zeros of the zeta function*, *Math. Comput.* **48**, 273 (1987).
- [65] J. Hadamard, *Sur la distribution des zéros de la fonction et ses conséquences arithmétiques*, *Bull. Soc. Math. France* **24**, 199 (1896).
- [66] H. L. Montgomery, *The pair correlation of zeros of the zeta function*, in *Proc. Symp. Pure Math*, Vol. 24 (1973) pp. 181–193.
- [67] E. Bombieri, *Problems of the millennium: The Riemann hypothesis*, (2000).
- [68] P. Cvitanovic, I. Percival, and A. Wirzba, *Quantum Chaos & Quantum Measurement*, Vol. 358 (Springer Science & Business Media, 2013).
- [69] T. Geisel, R. Ketzmerick, and G. Petschel, *New class of level statistics in quantum systems with unbounded diffusion*, *Phys. Rev. Lett.* **66**, 1651 (1991).
- [70] I. M. Sokolov, J. Klafter, and A. Blumen, *Fractional kinetics*, *Phys. Today* **55**, 48 (2002).
- [71] I. Guarneri and G. Mantica, *Multifractal energy spectra and their dynamical implications*, *Phys. Rev. Lett.* **73**, 3379 (1994).
- [72] V. G. Benza and C. Sire, *Band spectrum of the octagonal quasicrystal: Finite measure, gaps, and chaos*, *Phys. Rev. B* **44**, 10343 (1991).
- [73] L. Dal Negro and S. Inampudi, *Fractional transport of photons in deterministic aperiodic structures*, *Sci. Rep.* **7**, 2259 (2017).
- [74] Y. Chen, A. Fiorentino, and L. Dal Negro, *A fractional diffusion random laser*, *Sci. Rep.* **9**, 1 (2019).
- [75] M. Schreiber and H. Grussbach, *Multifractal wave functions at the Anderson transition*, *Phys. Rev. Lett.* **67**, 607 (1991).
- [76] M. Schreiber and H. Grussbach, *Fluctuations in mesoscopic systems*, *Philos. Mag. B* **65**, 707 (1992).
- [77] J. Pichard and G. Sarma, *Power-law decay and fractal character of eigenstates in two-dimensional disordered systems*, *J. Phys. Condens. Matter* **18**, 3457 (1985).
- [78] P. Sebbah, D. Sornette, and C. Vanneste, *Anomalous diffusion in two-dimensional Anderson-localization dynamics*, *Phys. Rev. B* **48**, 12506 (1993).
- [79] S. John, *Localization of light*, *Phys. Today* **44**, 32 (1991).